Three-component domains in fully hydrated Nafion membrane characterized by partial scattering function analysis

Yue Zhao,[1,*] Kimio Yoshimura,[1] Toshinori Motegi,[1] Akihiro Hiroki,[1] Aurel Radulescu,[2] Yasunari Maekawa[1,*]

[1]*Department of Advanced Functional Materials Research, Takasaki Advanced Radiation Research Institute, National Institutes for Quantum and Radiological Science and Technology (QST), Watanuki-machi 1233, Takasaki, Gunma, 370-1292, Japan*
[2]*Forschungszentrum Jülich GmbH, Jülich Centre for Neutron Science @ MLZ, Lichtenbergstraße 1, D-85747 Garching, Germany*

*To whom all correspondence should be addressed: Yue Zhao (zhao.yue@qst.go.jp); Yasunari Maekawa (maekawa.yasunari@qst.go.jp)

Three-component domains in fully hydrated Nafion membrane characterized by partial scattering function analysis

Yue Zhao, Kimio Yoshimura, Toshinori Motegi, Akihiro Hiroki, Aurel Radulescu, Yasunari Maekawa

for Table of Contents use only

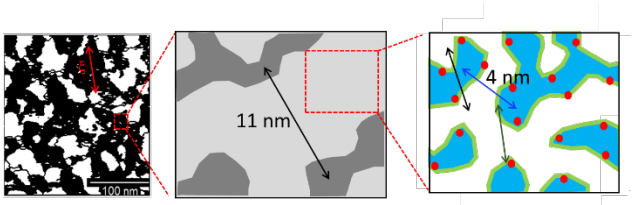

Abstract: A fully hydrated Nafion membrane is generally treated as a three-component system comprising the tetrafluoroethylene-like main-chain, the fluorinated side-chain ending with a sulfonic acid group, and absorbed water. We applied the contrast variation small-angle neutron scattering technique to decompose the scattering intensity profiles to partial scattering functions (PSFs) of each component in Nafion quantitatively. In the large-scale (>30 nm), structural heterogeneities were observed in the main- and side-chain domains but not in water domains. In the middle-scale (5 – 30 nm), bicontinuous-like structure of crystalline and amorphous phases with a mean separation distance of 11 nm was observed, as a result of the main-chain semicrystalline templating effect. In the small-scale (<5 nm), another bicontinuous-like structure exists in the amorphous phase with a mean separation distance of about 4 nm, indicating a well-connected water network responsible for the good membrane conductivity. Cross-term analysis of PSFs for two components suggested that the location of each component in that the main-chain domains tends to phase-separate from either the side-chain or water domains, but the side-chain and water domains are closely attached through sulfonic acid groups.

I. Introduction

Perfluorosulfonic acid polymer membranes, such as Nafion(T), are benchmark materials for a proton-exchange membrane and have been commercialized in residential and automobile fuel cells and electrolytic synthesis of chlorine and sodium hydroxide owing to their excellent proton conductivity and thermomechanical properties.[1–4] Nafion comprises a chemically inert tetrafluoroethylene (TFE)-like main-chain and pendant perfluoroalkyl ether (PFA) side-chains with sulfonic acid ionic groups ($-SO_3H$) at the terminal of the side-chains. Upon hydration, ionic groups absorb water and form hydrophilic ion-conducting nanodomains (ion channels), through which proton and water transport occurs, phase-separated from the semicrystalline hydrophobic polymer matrix.

Hydration-induced phase-separated morphology of Nafion membranes has been extensively studied in the past decades using small-angle X-ray scattering (SAXS) and neutron scattering (SANS).[1,4] The morphological analysis is mainly based on the scattering intensity profiles of $I(q)$ as a function of the scattering vector, q. Generally $I(q)$ of hydrated Nafion membranes shows three features in the representative q-regimes: i) a small-angle upturn at $q < 0.1$ nm^{-1} (>60 nm), ii) the first broad peak at $0.2 < q < 1.0$ nm^{-1} (6 – 30 nm), and iii) the second strong peak at $q > 1.0$ nm^{-1} (<6 nm). Although the detailed structure (such as size, shape, and connection) is still under debate and the quantitative assignment of the characteristic structure (such as the composition of the scattering objects) is ambiguous, it is generally accepted that the small-q upturn is related to large structures, the first peak is related to the intercrystalline spacing between the crystalline domains of the polymer matrix, and that the second peak (ionomer peak) arises from the correlation of hydrophilic water domains. The small-angle upturn and two peaks are usually interrelated, indicating that there exists a counterbalance between the

semicrystalline polymer matrix and hydrophilic water domains that governs the degree of phase-separation. The properties of the Nafion membrane are closely related to its hierarchical structures.

Numerous morphological models based on the $I(q)$ data have been proposed, especially for the strong ionomer peak, such as the cluster-network model where interconnected nanoscale spherical water clusters are distributed in the polymer matrix,[5,6] the sandwich model where water is embedded in the polymer matrix,[7] the disordered network of polymer chains and water pools,[8] the ribbon-like structure of polymer domains separated by water,[9] parallel cylindrical water nanochannels embedded in the polymer matrix,[10] a bicontinuous network of hydrophilic domains,[11] and a locally flat, layered structure of water domains.[12] There are also direct imaging approaches, *i.e.*, Allen *et al*. reported the first direct 3D nanoscale image of a fully hydrated as-cast Nafion membrane using Cryo-TEM tomography.[13] They revealed an interconnected channel-type network structure with a domain spacing of about 5 nm, which was similar to the bicontinuous model based on the scattering data.[11]

Notably, $I(q)$ profile of Nafion membrane contains scattering contributions from all components, *i.e.*, the main-chains, side-chains, and water. For such a complex system comprising more than two components, it is impossible to accurately identify the concrete structure of each component and the structural correlation of every two different components via the analysis on $I(q)$ alone. As such, the partial scattering functions (PSFs) of each component in the membrane must be analyzed, which can be achieved via the quantitative decomposition of a series of $I(q)$ obtained through the contrast variation SANS technique,[14] which is based on hydrogen/deuterium replacement to modify the scattering visibility (*i.e.*, contrast) of the components in the system. In other words, the

contrast variation ensures no change in the native structure of each component, but changes in its contribution to the final scattering intensity. The quantitative decomposition of scattering intensity profiles of a ternary system into PSFs has been theoretically developed, and successfully applied to polymer nanocomposites,[15–19] rubber-filled systems,[20] catalyst ink,[21–23] *etc*. The most-difficult aspects of this technique are the accurate determination of the scattering length density (SLD) of each component and precise control of the scattering contrast. These difficulties can be solved in the hydrated Nafion membrane because of the following two reasons. First, the chemical structure of Nafion is clearly known, which allows for the theoretical SLD calculation of each component. Second, the scattering contrast can be precisely controlled by varying the absorbed water composition that is composed of H_2O and D_2O with different volume ratios.

Traditionally, structure analysis of Nafion relies on the scattering intensity profile, which can only qualitatively give the possible structure images of all components, but not the quantitative structure information of each component in the membrane. To understand the exact structure and location of each component, PSF profiles are preferred over the scattering intensity profiles.[14, 24]

In this study, we use PSF analysis to identify the detailed structure of each component (*i.e.*, main-chain, side-chain, and water), and the structural correlation between two components to determine the hierarchical structures of hydrated Nafion (i.e. bicontinuous, flat layered, or ribbon-like structures).

II. Experimental details

II-1 Materials

Nafion membrane (NR-212, mass density = 1.97 g/cm^3) with a thickness of 50.8 μm

was purchased from DuPont. Before the experiment, the membranes were sequentially immersed in 3 wt% hydrogen peroxide solution, deionized water (H_2O), 1 M sulfuric acid, and then deionized water at 80 ℃ for 1 h in each process. Hydrogen peroxide aqueous solution (30 wt%) and 1-M sulfuric acid were purchased from FUJIFILM Wako Pure Chemical Co. Deionized water was purified using a Millipore Milli-Q UV system to produce water with a resistance of 18.2 MΩ·cm and a total organic carbon content of <10 ppb. Deuterated water (D_2O, 99.9 atom% D) used in SANS experiments was purchased from Sigma-Aldrich Co. Ltd.

II-2. Small-angle neutron scattering measurement

SANS measurements were performed on KWS-2 SANS diffractometer operated by Juelich Centre for Neutron Science at the neutron source Heinz Maier–Leibnitz (FRM II reactor) in Garching, Germany.[25] The incident neutron beam at KWS-2 was monochromatized with a velocity selector to have the average wavelength (λ) of 5 Å with a wavelength resolution of $\Delta\lambda/\lambda$= 20%. The scattering patterns were collected using a two-dimensional (2D) scintillation detector and circularly averaged to obtain scattering intensity profiles as a function of q, where q is the scattering vector and defined as $q = (4\pi/\lambda)\sin(\theta/2)$, where θ is the scattering angle. The final obtained intensity profiles were corrected for the background of the cell, electronic noise of the detector, detector sensitivity, and incoherent scattering. All measurements were performed at 25 ± 0.5 ℃.

II-2. Decomposition of scattering intensity profiles into Partial scattering functions

The quantitative decomposition of scattering intensity profiles of a ternary system into PSFs has been detailed in section S1 in the supporting information and in ref. 15-23, and here we simply mention the main results under the incompressibility assumption, which is applied to most condensed systems. The scattering intensity profiles can be

described using three PSF self-terms[14, 17]

$$I(q) = (b_1 - b_2)(b_1 - b_3)S_{11}(q) + (b_2 - b_1)(b_2 - b_3)S_{22}(q) + (b_3 - b_1)(b_3 - b_2)S_{33}(q) \quad (1)$$

where b_i and S_{ii} are the SLD and PSF self-term of the i component ($i = 1 - 3$). S_{ii} is defined as[24]

$$S_{ii}(q) = \frac{1}{V} < \iint \delta\varphi_i(\vec{\mathrm{r}})\delta\varphi_i\left(\overrightarrow{\mathrm{r}'}\right) \exp\left[-i\vec{q}\left(\vec{\mathrm{r}} - \overrightarrow{\mathrm{r}'}\right)\right] d\vec{\mathrm{r}} d\overrightarrow{\mathrm{r}'} > \quad (2)$$

where V is the scattering volume and $\delta\varphi_i(\vec{\mathrm{r}})$ is the fluctuation part of the volume fraction of the i component at position $\vec{\mathrm{r}}$ ($\varphi_i(\vec{\mathrm{r}})$), which is expressed as

$$\delta\varphi_i(\vec{\mathrm{r}}) = \varphi_i(\vec{\mathrm{r}}) - \bar{\varphi}_i \quad (3)$$

where $\bar{\varphi}_i$ is the average volume fraction of the i component (*i.e.*, $\bar{\varphi}_i = \frac{1}{V}\int \varphi_i(\vec{\mathrm{r}})d\vec{\mathrm{r}}$). The definition in Eq. (2) indicates that $S_{ii}(q)$ is the Fourier transform of the correlation function of $\delta\varphi_i(\vec{\mathrm{r}})$, $\gamma_i(\vec{\mathrm{u}})$, which is given by

$$\gamma_i(\vec{\mathrm{u}}) = \int \delta\varphi_i(\vec{\mathrm{r}})\delta\varphi_i(\vec{\mathrm{r}} + \vec{\mathrm{u}})d\vec{\mathrm{r}} \quad (4)$$

As $\gamma_i(\vec{\mathrm{u}})$ specifies how $\delta\varphi_i(\vec{\mathrm{r}})$ and $\delta\varphi_i\left(\overrightarrow{\mathrm{r}'}\right)$ in neighboring regions separated by $\vec{\mathrm{u}}$ correlate with each other in the real space, it gives the structural information of the i component. The details of S_{ii} as a function of q can be experimentally determined from the intensity profiles obtained from the contrast-variation SANS experiments as shown in section S2 in the supporting information.[14, 17]

The PSF cross-term S_{ij} ($i \neq j$), defined by the following equation

$$S_{ij}(q) = \frac{1}{V} < \iint \delta\varphi_i(\vec{\mathrm{r}})\delta\varphi_j\left(\overrightarrow{\mathrm{r}'}\right) \exp\left[-i\vec{q}\left(\vec{\mathrm{r}} - \overrightarrow{\mathrm{r}'}\right)\right] d\vec{\mathrm{r}} d\overrightarrow{\mathrm{r}'} > \quad (5)$$

can be deduced from S_{ii} using Eqs (6) – (8) under the incompressibility assumption.[14, 17]

$$S_{12} = \frac{1}{2}(S_{33} - S_{11} - S_{22}) \quad (6)$$

$$S_{23} = \frac{1}{2}(S_{11} - S_{22} - S_{33}) \quad (7)$$

$$S_{13} = \frac{1}{2}(S_{22} - S_{11} - S_{33}) \quad (8)$$

II-3. Atomic force microscopy

Atomic force microscopy (AFM) measurements were performed on an AFM5300E (Hitachi High-Tech Science Corporation, Tokyo, Japan) equipped with an open-loop scanner (scan range: 20 μm × 20 μm × H1.5 μm). Standard, commercially available Si_3N_4 cantilevers with integrated tips were used as AFM probes. The tips had a radius of curvature of 10 nm and a spring constant of 1.6 N/m as supplied by the manufacturer. After the pretreatment, Nafion membranes were allowed to air-dry and mounted on the sample stage using double-sided tape. All AFM measurements of the Nafion surface were performed under ambient conditions at room temperature under a relative humidity range of 20%–30%. For image analysis, the open-source software, Gwiddion, was employed.[26] The characteristic size of the polymer structure was calculated from the radial averaged power spectrum obtained from 2D-FFT operation following the watershed binarization process.[27]

III. Results

III-1 Contrast variation SANS

Contrast variation SANS measurements were performed on a Nafion 212 membrane equilibrated in H_2O/D_2O mixture with nine different D_2O volume fractions (f_{D2O}). The scattering intensity profiles, $I(q)$, at the representative H_2O/D_2O volume ratios are shown in Figure 1. In agreement with the previously reported scattering features, the small-q upturn and two scattering peaks are observed in all $I(q)$ profiles. The small-q upturn follows the power-law relationship with an exponent increasing from −1 to approximately

−4 with f_{D2O} at $f_{D2O} > 70\%$. The first scattering maximum appears at $q_1 = 0.53$ nm^{-1}, and the corresponding d-spacing ($2\pi/q_1$) is 11.8 nm. The peak intensity decreases with increasing f_{D2O} at $f_{D2O} < 77\%$ without a change in the peak shape and width, exhibiting the minimum value at $f_{D2O} = 90\%$ and then increases again at $f_{D2O} = 100\%$. The second scattering peak appears at $q_2 = 1.44$ nm^{-1}, with the corresponding d-spacing ($2\pi/q_2$) being 4.3 nm. Similar to the first peak, its intensity also first decreases and then increases with increasing f_{D2O}, but at a different transition point at $f_{D2O} = 77\%$.

According to Babinet's principle,[14, 24] if the system comprises only two components, contrast variation experiments will only change the absolute intensity but not the shape of the scattering profiles (see section S1 in the supporting information). Therefore, the fully hydrated Nafion membrane is not evidenced as a simple "two-component" system. Thus, the structural analysis merely based on $I(q)$ cannot provide the accurate structure of each component in the membrane quantitatively. Therefore, in the following section, we introduce PSF analysis.

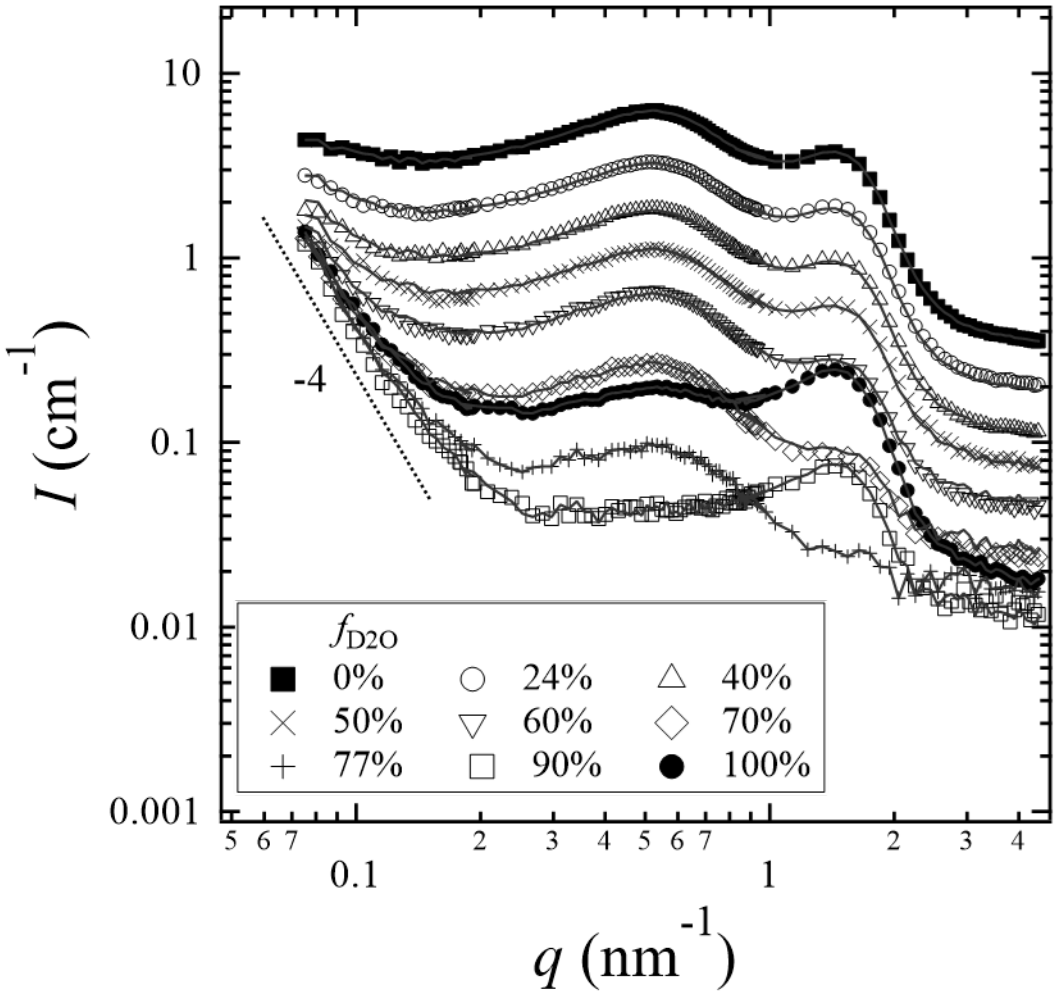

Figure 1 Experimental scattering intensity profiles (symbols) and the reconstructed intensity profiles (solid lines) of the fully hydrated Nafion membrane swollen in water mixtures of D_2O and H_2O with different ratios.

III-2 Partial scattering function analysis

We treat the hydrated Nafion membrane as a three-component system. The fluorinated main-chain of Nafion [$–(C_2F_4)_m–C_2F_3–$ with $m \cong 6.5$ for NR-212] is hydrophobic, which should be phase-separated from water. Therefore, the Nafion membrane is partitioned into separate components of the main-chain, whole side-chain ($C_5F_{10}O_2–SO_3H$), and water (Scheme 1). The SLD of each component can be calculated

on the basis of the chemical structure and mass density.[24, 28] Theoretically determined SLDs of the main-chain (b_{MC}) and side-chain (b_{SC}) are listed in Table 1. SLD of water (b_W) varies as a function of f_{D2O} of the water mixture:

$$b_W = b_{D2O} f_{D2O} + b_{H2O}(1 - f_{D2O}) \qquad (9)$$

where b_{D2O} and b_{H2O} are the SLD of D_2O and H_2O being 6.34 and −0.56 ($\times 10^{10}$ cm^{-2}), respectively.[24, 28, 29]

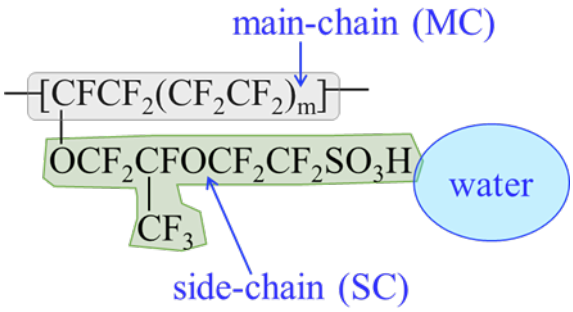

Scheme 1 Illustration of the three-component system of the fully hydrated Nafion composed of the main-chain (MC), side-chain (SC) and water.

Table 1 SLD (b_x) of each component in the fully hydrated Nafion membrane.

Components	Main-chain	Side-chain	Water
b_x ($\times 10^{10}$ cm^{-2})	4.34	3.73	Variable

Thus Eq. (1) can be rewritten to

$$I(q) = (b_{MC} - b_{SC})(b_{MC} - b_W)S_{MC-MC}(q) + (b_{SC} - b_{MC})(b_{SC} - b_W)S_{SC-SC}(q) + (b_W - b_{MC})(b_W - b_{SC})S_{W-W}(q) \qquad (10)$$

where i = MC: main-chain, SC: side-chain, and W: water, for the current hydrated Nafion membrane. The PSF cross-terms S_{ij} are rewritten to

$$S_{MC-SC} = \frac{1}{2}(S_{W-W} - S_{MC-MC} - S_{SC-SC}) \qquad (11)$$

$$S_{SC-W} = \frac{1}{2}(S_{MC-MC} - S_{SC-SC} - S_{W-W}) \qquad (12)$$

$$S_{MC-W} = \frac{1}{2}(S_{SC-SC} - S_{MC-MC} - S_{W-W}) \qquad (13)$$

The self-term S_{ii} reflects the exact structure of the i component, while the cross-term S_{ij} ($i \neq j$) gives information about the interaction between the i and j components and their positions relative to each other. Thus, in the following sections, we analyze the self-terms and cross-terms of PSFs.

III-2.1 Self-terms

Three self-terms of PSFs, including main-chain ($S_{MC\text{-}MC}$), side-chain ($S_{SC\text{-}SC}$), and water ($S_{W\text{–}W}$) are plotted as a function of q in Figure 2. All the SANS intensity profiles were reconstructed via backsubstitution with three self-terms of PSFs using Eq. (10). The reconstructed $I(q)$ profiles (solid lines) are well matched to the experimental profiles (symbols) as shown in Figure 1, indicating the correctness of S_{ii} with the appropriate SLDs, *i.e.*, the validity of the application of the PSF method to the Nafion sample.

As shown in Figure 2, the absolute value of S_{ii} in the order of $S_{MC\text{–}MC} > S_{SC\text{–}SC} > S_{W\text{–}W}$ in the whole-q range means that the magnitude of correlation functions of main-chain, side-chain, and water follow the same trend of $\gamma_{MC-MC} > \gamma_{SC-SC} > \gamma_{W-W}$ in the real space. Therefore, we can conclude that the main-chain dominantly contributes to the structure pattern more than the other two components, i.e., the main-chain works as a template in the membrane.

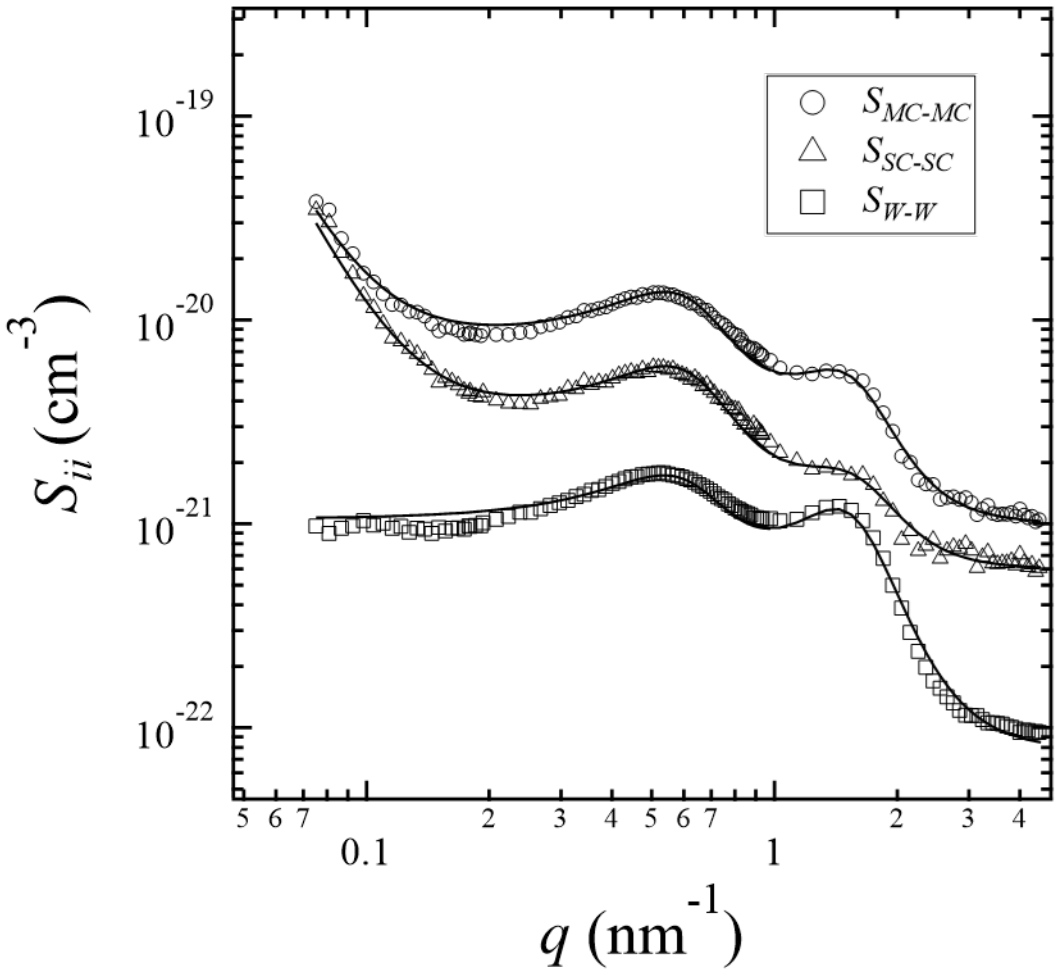

Figure 2 PSF self-terms of the fully hydrated Nafion (symbols) and the best-fitting results obtained using Eq. (14) (solid lines). The fitting parameters are listed in Table 3.

In addition, the following structural features are observed in S_{ii}. In the small-q regime at $q < 0.2$ nm^{-1}, either S_{MC-MC} or S_{SC-SC} exhibits an upturn with a power-law exponent of −4, indicating that the main-chain and side-chain components are not homogeneously distributed in this length scale. By contrast, no small-q upturn in S_{W-W} is observed, indicating that water is homogeneously distributed in this length scale. In the middle-q regime at 0.2 nm^{-1} < q < 1 nm^{-1}, S_{MC-MC}, S_{SC-SC}, and S_{W-W} show a broad peak with a center

position close to the crystalline peak observed in the scattering intensity profiles (Figure 1). The shape and sharpness of the peak in all S_{ii} are similar, reflecting the similar structure. In the high-q regime at $q > 1$ nm^{-1}, S_{MC-MC}, S_{SC-SC}, and S_{W-W} show a peak with the center position close to the ionomer peak observed in the scattering intensity profiles but a relatively broader peak is observed in S_{SC-SC} compared to S_{MC-MC} and S_{W-W}.

Sugiyama *et al.* obtained the PSF self-term of Cu ions (S_{Cu-Cu}), which were absorbed in Nafion membrane in a limited q-range of $0.35 < q < 2.5$ nm^{-1}, using a small-angle X-ray scattering method with X-ray anomalous dispersion effect.[30] They revealed the hierarchical distribution of hydrophilic domains where Cu ions are located. Though a detailed structural analysis of $S_{Cu\text{-}Cu}$ profile was not performed in that study, we find that S_{Cu-Cu} is quite similar to S_{W-W} observed in Figure 2. Note that the PSF self-term of each component cannot be directly extracted using the anomalous X-ray scattering method.

III-2.2 Cross-terms

Using contrast variation SANS, it is possible to evaluate the PSF cross-terms S_{ij} ($i \neq j$) through Eqs. (11)–(13), which reflect cross-correlations between the components i and j, as defined in Eq. (5). The sign of S_{ij} reveals the interaction force between i and j, *i.e.,* positive and negative signs of Sij indicate attractive and repulsive interactions, respectively. The shape of S_{ij} profiles indicate the geometry distribution of the two components.[14]

Figure 3 shows the calculated PSF cross-terms of S_{MC-SC}, S_{MC-W}, and S_{SC-W} as a function of q. S_{MC-SC} and S_{MC-W} are negative, indicating the repulsive interactions between the main- and side-chains, and between main-chains and water. S_{SC-W} is found to be positive with a noticeable magnitude in comparison with S_{SC-SC} and S_{W-W}, as shown in the inset of Figure 3, suggesting a strong attractive interaction between the side-chain and

water.

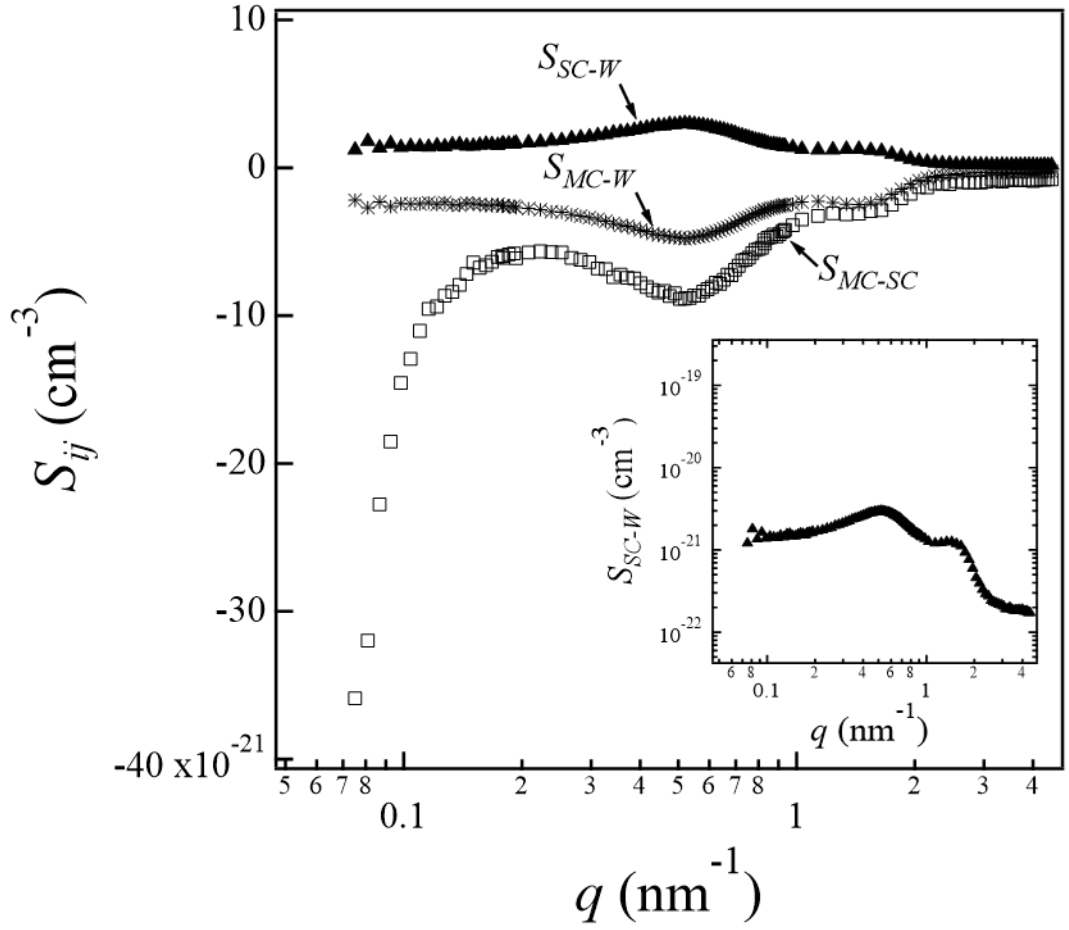

Figure 3 PSF cross-terms of the fully hydrated Nafion. The inset shows the plot of $S_{SC\text{-}W}$ in the logarithmic scale.

III-3. Structural analysis on S_{ii} using Debye–Bueche and Teubner–Strey models

As already mentioned, S_{ii} contains the structural information of the i component, which comprises three parts: upturn/or-not in the small-q regime at $q < 0.2$ nm^{-1}, one peak in the middle-q regime at 0.2 nm^{-1} $< q <$ 1 nm^{-1}, and another peak in the high-q regime at $q > 1$ nm^{-1}. We use the Debye–Bueche (DB) model to describe the small-q upturn and the Teubner–Strey (TS) model to fit the peaks in the middle- and high-q regimes (Table 2). Thus, S_{ii} is constructed as the sum of the three-model analysis:

$$S_{ii}(q) = C_1 S_{DB}(q) + C_2 S_{TS,1}(q) + C_3 S_{TS,2}(q) + C_B \qquad (14)$$

where C_1, C_2, and C_3 are the fitting constants, and C_B is the constant background. The first term, $S_{DB}(q)$, is the scattering function of DB model:

$$S_{DB}(q) \sim \frac{8\pi\xi^3}{(1+q^2\xi^2)^2} \qquad (15)$$

where ξ is the characteristic size. $S_{DB}(q)$ is generally applied to two-phase systems, in which one phase is randomly distributed in another phase, such as the "island-and-sea" structure having a characteristic "island" size of ξ, as schematically shown in Figure S1(a) in the supporting information.[31, 32] The second term $S_{TS,1}(q)$ and third term $S_{TS,2}(q)$ are scattering functions of TS model describing bicontinuous-shaped morphology of the domains,[33–36] which correspond to the first and second peaks in the middle- and high-q regimes, respectively. $S_{TS}(q)$ is generally expressed as follows:

$$S_{TS}(q) \sim \frac{8\pi d^4}{\varepsilon[16\pi^4 + 8d^2\pi^2(\varepsilon^{-2} - q^2) + d^4(\varepsilon^{-2} + q^2)]} \qquad (16)$$

where d is the mean distance between two domains and is determined from the peak position, q_m ($d = 2\pi/q_m$), and ε is considered as the dispersion of d (inversely proportional to the peak width). Thus, a broader peak leads to a smaller ε, thus indicating a more disordered bicontinuous structure with less interfacial correlations. The schematic pictures of TS models with similar d values but different ε values are illustrated in Figure S1(b) and S1(c) in the supporting information.

The best-fitted curves obtained using Eq. (14) are shown together with S_{ii} in Figure 2. The fitting parameters, i.e., ξ from the DB model and the two sets of d and ε values from the TS model, namely, d_1 and ε_1 in $S_{TS,1}(q)$ and d_2 and ε_2 in $S_{TS,2}(q)$, respectively, are listed in Table 3.

Table 2 Summary of hierarchical structures of each component by model analysis

q-regime	Fitting model	Structure of the component		
		MC	SC	W
Small-q	DB model	Heterogeneous	Heterogeneous	Homogeneous
Middle-q	TS model	Bicontinuous	Bicontinuous	Bicontinuous
High-q	TS model	Bicontinuous	Bicontinuous	Bicontinuous

Table 3 Best-fitting parameters of the DB-model and two TS-models

S_{ii}	ξ (nm)	d_1 (nm)	ε_1 (nm)	d_2 (nm)	ε_2 (nm)
$S_{MC\text{-}MC}$	>65	10.7	4.1	4.2	2.0
$S_{SC\text{-}SC}$	>65	10.7	4.1	4.0	1.7
$S_{W\text{-}W}$	-	10.8	4.2	4.2	2.1

III-4 Direct observation using AFM

We performed direct observation on the surface of Nafion-212 membrane using AFM technique to obtain the topographic image of a 500 nm × 500 nm (512 pixel^2) area (Figure 4). The image was analyzed to obtain the radial averaged power spectrum via 2D-FFT operation (Figure 4). The power spectrum indicates the most probable characteristic correlation distance of 112 nm. As phase-contrast imaging can provide fine details about phase separated structures in polymer solids even with rough surfaces, we measured a phase-contrast image in an area of 250 nm × 250 nm (256 pixel^2), as shown in Figure 5(a).[37] The correlation distance of 10.6 ± 0.28 nm (number of images = 3) in the corresponding power spectrum was obtained as a characteristic size of the fine structure, which is in good agreement with the periodical distance (8.2 ± 0.8 nm) evaluated from the phase-contrast image in Figure 5(b).

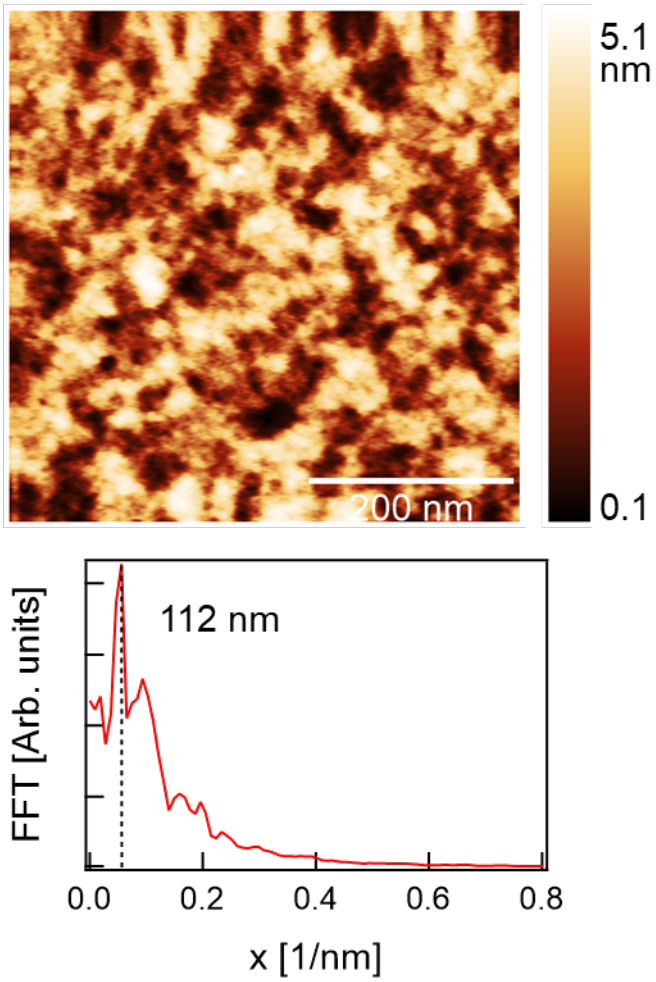

Figure 4 AFM full-size topographic image of Nafion surface. The image is shown with the averaged radial power spectrum calculated from the 2D FFT operation.

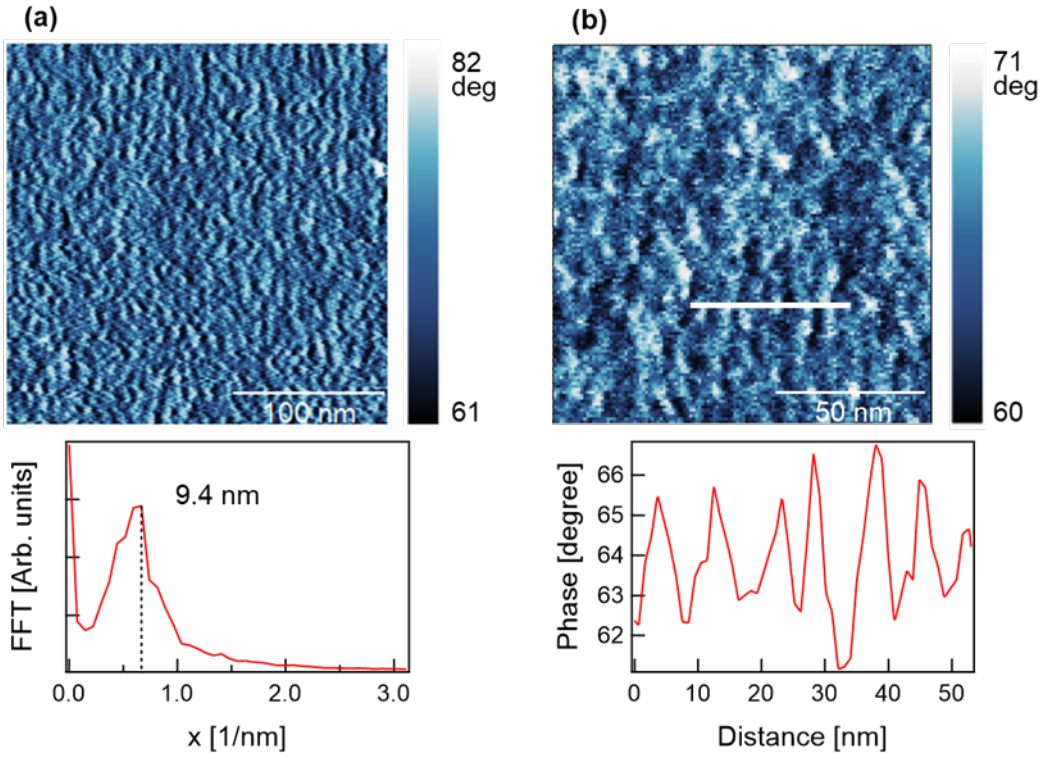

Figure 5 (a) Typical AFM phase-contrast image, and the radial power spectrum calculated from the 2D FFT operation. (b) Enlarged phase-contrast image, and the obtained periodical distance profile along the white line in the image.

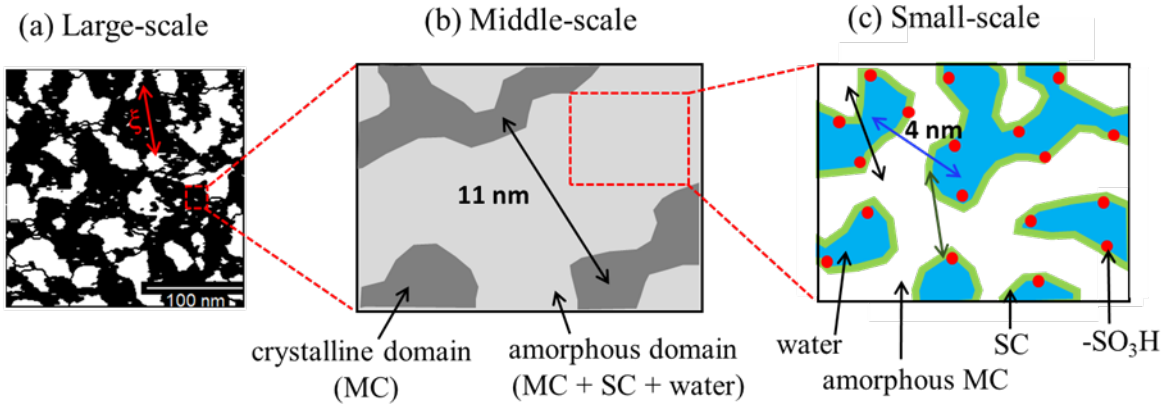

Figure 6 Schematic of the hierarchical structure of the main-chain, side-chain and water domains in the fully hydrated Nafion membrane at (a) large-scale; (b) middle-scale; and (c) small-scale.

IV. Discussion

Small-*q* regime. DB-model analysis on S_{MC-MC} and S_{SC-SC} shows that both the main-chain and side-chain have large-scale structure heterogeneities with a size of $\xi > 65$ nm, which is in agreement with the characteristic size observed in AFM topographic images shown in Figure 4. This large-scale structural heterogeneity is believed to originate from two domains, both of which comprise the main- and side-chain of Nafion with water but possess different ratios of the main- to side-chains. As the TFE (main chain) and PFA (side chain) units are randomly arranged, one domain with the sequence that includes more TFE units can form more semicrystalline structures than the other domain that has less main-chain, resulting in less semicrystalline structures. Figure 6(a) shows the schematic picture of the large-scale structure, drawn based on the AFM observation. The similar ξ values for the main-chain and side-chain components are reasonable because the two components are chemically linked, which results in coordinative movements. In other words, the ξ values for main-chain and side-chain components should correspond to the fluctuation of the longer sequence of crystalline TFE units in the Nafion polymer chains.

On the contrary, the third component, water, is distributed more or less homogeneously in both semicrystalline (main-chain)- and amorphous (side-chain)- rich domains, resulting in the plateau part of S_{W-W} in the small-*q* regime. This new finding is remarkably advanced than the traditional structural analysis based on the scattering intensity profile, e.g., the low-*q* intensity scales with $I(q) \sim q^{-\alpha}$ ($-1 \leq \alpha \leq -2$) were reported, but accurate assignment for either the main-chain, side-chain or water was missing.[4] The structural feature of homogeneous distribution of water in large-length scale is found in this study for the first time using the contrast variation SANS technique

and the delicate PSF analysis. Such a unique water structure is believed to cause the high conductivity of the hydrated Nafion membrane.

Middle-*q* regime. From the TS-model analysis of S_{MC-MC}, S_{SC-SC} and S_{W-W}, we observed that all components exhibit similar bicontinuous-like structures with similar d_1 (ca. 11 nm) and ε_1 (4.1 – 4.2 nm) values. Note that the side-chains and water are located in the amorphous phase of the main-chain, while the crystalline phase of the main-chain remains nonhydrated. Thus, the main-chain crystalline domains are phase-separated from the amorphous domains. The d_1 value of S_{MC-MC} represents the characteristic separation distance of the two main-chain crystalline domains. Similar d_1 values are observed for both S_{SC-SC} and S_{W-W} because the side-chain with water in hydrophilic domains are structured through the influence of the semicrystalline main-chain matrix. Thus, the selective distribution of side-chains and water, together with the semicrystalline feature of main-chains are the main factors for the similar bicontinuous structure of all components in the middle-*q* regime. AFM phase-contrast image also shows a characteristic length of 9.4 nm (Figure 5(a)), which is in good agreement with the d_1 value determined from S_{ii}. A schematic of the structure in the middle-scale is shown in Figure 6(b).

High-*q* regime. S_{MC-MC}, S_{SC-SC} and S_{W-W} profiles at high-*q* regime can also be well fitted using the TS-model, indicating that all components have bicontinuous-like local structures with similar d_2 value (4.0 – 4.2 nm). However, the ε_2 value of side-chain (ca. 1.7 nm) is found to be smaller than that of the main-chain (ca. 2.0 nm) and water (ca. 2.1 nm), which can be observed from the broader peak of S_{SC-SC} compared to S_{MC-MC} and S_{W-W} in the high-*q* regime. Thus, the local structure of the side-chain domains is more disordered than that of the main-chain and water domains probably because side-chains,

which are chemically linked to the main-chain at one end and physically linked to water at the other end, locate at the interface of hydrophobic main-chain phase and hydrophilic water phase, making the interface of domains more vague.

All the components can be allocated via the analysis of S_{ij} in Figure 3. The negative S_{MC-SC} and S_{MC-W} indicate that the main-chain domains tend to phase-separate from both side-chain domains and water domains. S_{SC-W} is found to be positive and comparable with S_{SC-SC} and S_{W-W}, suggesting a strong attachment between the side-chain and water. This is because the side-chain is ending with a hydrophilic sulfonic acid group, which can strongly absorb water. Thus, it is reasonable to image the picture in which the side-chain and water domains are closely attached via sulfonic acid groups at the interface of two domains. The profile shape of S_{SC-W} in Figure 3 is similar to that of S_{SC-SC} and S_{W-W} in Figure 2, indicating that the strong attachment between side-chain and water does not result in structural distortion to either side-chain or water domains, partly because the interaction of side-chain and water domains mainly exists in the interface, and partly because the structures of both side-chain and water domains are robust. Thus, the detailed local structure and location of all the components are pictured and schematically shown in Figure 6(c), which clearly indicates that the distribution of side-chain domains is influenced by both main-chain and water domains, thus confirming the above explanation for the more disordered side-chain local structure.

V. Conclusions

We studied the structure of fully hydrated Nafion membranes by performing contrast variation SANS experiments, which allows for the decomposition of the scattering intensity data into PSFs of each component. These PSFs are essential for the quantitative understanding of the role of each component in the whole structure.

Our results confirmed the validity of three-component domains of the main-chain, the side-chain and water. The analysis of PSF self-terms revealed the detailed structure of each component, and that of the cross-terms gave the correlation between two components leading to the location determination of the component. The whole structure pattern of the hydrated Nafion membrane was constructed (Figure 6); the main-chain forms the bicontinuous-shaped template made of crystalline main-chain and amorphous domains with side-chain and water distributed in the amorphous domains. All components have a bicontinuous-like local structure. Main-chain and side-chain show heterogeneity in the large-scale with a size of >65 nm; however, water distributes homogeneously in the large-scale, indicating the formation of well-connected network which is believed to be the key structural factor for high membrane conductivity.

Notes

The authors declare no competing financial interest.

Acknowledgments

This work was partially supported by Grant-in-Aid for Scientific Research (A) from Japan Society for the Promotion of Science (JSPS) (KAKENHI Grant Number: 18H03850), and partially supported by "Advanced functional polymer materials alliance" project under QST innovation hub program in collaboration with participant companies, and "FY2020 Diversity Promotion Collaborative Research Subsidy" by the Diversity Promotion Office in QST.

Supporting information

Incompressibility assumption and Babinet's principle for a ternary system; Decomposition of scattering intensity profiles into partial scattering functions by contrast variation; Schematic of the morphology described by DB model and TS model

References.

1. Maurtiz, H. A.; Moore, R. B. State of understanding of Nafion, *Chem. Rev.* **2004**, *104*, 4535-4585.
2. Hickner, M. A.; Pivovar, B, S. The chemical and structural nature of proton exchange membrane fuel cell properties, *Fuel Cells* **2005**, *5*, 213-229.
3. Hamrock, S. J.; Yandrasits, M. A. Proton exchange membranes for fuel cell applications, *J. Macromol. Sci., Part C: Polym. Rev.* **2006**, *46*, 219-244.
4. Kusoglu, A.; Weber, A. Z. New insights into perfluorinated sulfonic-acid ionomers, *Chem. Rev.* **2017**, *117*, 987-1104.
5. Gierke, T. D.; Munn, G. E.; Wilson, F. C. The morphology in Nafion perfluorinated membrane products, as determined by wide- and small-angle x-ray studies, *J. Polym. Sci., Polym. Phys. Ed.* **1981**, *19*, 1687-1704.
6. Gebel, G. Structural evolution of water swollen perfluorosulfonated ionomers from dry membrane to solution, *Polymer* **2000**, *41*, 5829-5838.
7. Haubold, H. G.; Vad, T.; Jungbluth, H.; Hiller, P. Nanostructure of Nafion: A SAXS study, *Electrochim. Acta* **2001**, *46*, 1559-1563.
8. Kim, M. H.; Glinka, C. J.; Grot, S. A.; Grot, W. G. SANS study of the effects of water vapor sorption on the nanoscale structure of perfluorinated sulfonic acid (Nafion) membranes, *Macromolecules* **2006**, *39*, 4775-4787.
9. Termonia, Y. Nanoscale modeling of the structure of perfluorosulfonated ionomer membranes at varying degrees of swelling, *Polymer* **2007**, *48*, 1435-1440.
10. Schmidt-Rohr, K.; Chen, Q. Parallel cylindrical water nanochannels in Nafion fuel-cell membranes, *Nat. Mater.* **2008**, *7*, 75-83.

11. Elliott, J. A.; Wu, D. S.; Paddison, S. J.; Moore, R. B. A unified morphological description of Nafion membranes from SAXS and mesoscale simulations, *Soft Matter* **2011**, *7*, 6820-6827.
12. Kreuer, K. D.; Portale, G. A critical revision of the nano-morphology of proton conducting ionomers and polyelectrolytes for fuel cell applications, *Adv. Funct. Mater.* **2013**, *23*, 5390-5397.
13. Allen, F. I.; Comolli, L. R.; Kesoglu, A.; Modestino, M. A.; Minor, A. M.; Weber, A. Z. Morphology of hydrated as-cast Nafion revealed through Cryo electron tomography, *ACS Macro Lett.* **2015**, *4*, 1-5.
14. Shibayama, M. Chapter 8 Soft Condensed Matter, *Experimental Methods in the Physical Sciences, Neutron Scattering-applications in biology, chemistry and materials science,* edited by Fernandez-Alonso, F. and Price D. L., **2017**, *46*, 459-546.
15. Richter, D.; Schneiders, D.; Monkenbusch, M.; Willner, L.; Fetters, L. J.; Huang, J. S.; Lin, M. Polymer aggregates with crystalline cores: the system polyethylene-poly(ethylenpropylene), *Macromolecules* **1997**, *30*, 1053-1068.
16. Poppe, A.; Willner, L.; Allgaier, J.; Stellbrink, J.; Richter, D. Structural investigation of micelles formed by an amphiphilic PEP-PEO block copolymer in water, *Macromolecules* **1997**, *30*, 7462-7471.
17. Endo, H.; Schwahn, D.; Colfen, H. On the role of block copolymer additives for calcium carbonate crystallization: small angle neutron scattering investigation by applying contrast variation, *J. Chem. Phys.* **2004**, *120*, 9410-9423.
18. Endo, H.; Miyazaki, S.; Haraguchi, K.; Shibayama, M. Structure of nanocomposite hydrogel investigated by means of contrast variation small-angle neutron scattering, *Macromolecules* **2008**, *41*, 5406-5411.

19. Matsunaga, T.; Endo, H.; Takeda, M., Shibayama, M. Microscopic structure analysis of clay-poly(ethylene oxide) mixed solution in a flow field by contrast-variation small angle neutron scattering, *Macromolecules* **2010**, *43*, 5075-5082.
20. Takanaka, M.; Nishitsuji, S.; Amino, N.; Ishikawa, Y.; Yamaguchi, D., Koizumi, S Structure analyses of swollen rubber-filler systems by using contrast variation SANS, *Macromolecules* **2009**, *42*, 308-311.
21. Kusano, T.; Hiroi, T.; Amemiya, K.; Ando, M.; Takahashi, T.; Shibayama, M. Structural evolution of a catalyst ink for fuel cells during the drying process investigated by CV-SANS, *Polymer J.* **2015**, *47*, 546-555.
22. Shibayama, M.; Matsunaga, T.; Kusano, T.; Amemiya, K.; Kobayashi, N.; Yoshida, T. SANS studies on catalyst ink of fuel cell, *J. Appl. Polym. Sci.* **2014**, *131*, 39842.
23. Yoshimune, W.; Harada, M. Effect of Pt loading on the adsorption of perfluoro-sulfonic acid ionomer in catalyst ink for polymer electrolyte fuel cells, *Chem. Lett.* **2019**, *48*, 487-490.
24. See for example, Roe, R. J. *Methods of X-ray and neutron scattering in polymer science*; Oxford Uni. Press: New York, 2000.
25. Radulescu, A.; Pipich, V.; Frielinghaus, H.; Appavou, M. S. KWS-2, the high intensity / wide Q -range smallangle neutron diffractometer for soft-matter and biology at FRM II, *Journal of Physics: Conference Series* **2012**, *351*, 012026.
26. Nečas, D.; Klapetek, P. Gwyddion: an open-source software for SPM data analysis, *Cent. Eur. J. Phys.* **2012**, *10*, 181–188.
27. Rabbani, A.; Ayatollahi, S. Comparing three image processing algorithms to estimate the grain-size distribution of porous rocks from binary 2D images and sensitivity

analysis of the grain overlapping degree, *Spec. Top. Rev. Porous Media* **2015**, *6*, 71-89.

28. SLD of a component with molecules composed of *i* atoms, can be calculated from the expression given by $SLD = (\frac{dN_A}{M_w}) \sum_i b_i$, where b_i is the scattering length of *i*th atom, d is the mass density of the component, M_w is the molecular weight, and N_A is the Avogadoro constant. The mass densities of TFE backbone and SO_3H are supposed to be 2.0 (Sigma-Aldrich) and 2.3 (ChemSpider) g/cm^3, respectively. Thus the mass density of side chain ($C_5F_{10}O_2$-SO_3H) is calculated to be 1.9 g/cm^3, in terms of the mass density of dry Nafion membrane being 1.97 g/cm^3. SLD of a component can be estimated with the knowledge of abovementioned mass density and its molecular structure.
29. Zhao, Y.; Yoshimura, K.; Shishitani, H.; Yamaguchi, S.; Tanaka, H.; Koizumi, S.; Szekely, N.; Radulescu, A.; Richter, D.; Maekawa, Y. Imidazolium-based anion exchange membranes for alkaline anion fuel cells: elucidation of the morphology and the interplay between morphology and properties, *Soft Matter* **2016**, *12*, 1567-1578.
30. Sugiyama, M.; Mitsui, T.; Sato, T.; Akai, Y.; Soejima, Y.; Orihara, H.; Na, Y. H.; Itoh, K.; Mori, K.; Fukunaga, T. Structural analysis of polyelectrolyte film absorbing metal ion by SAXS utilizing with X-ray anomalous dispersion effect, *J. Phys. Chem. B* **2007**, *111*, 8663-8667.
31. Debye, P.; Bueche, A. M. Scattering by an inhomogeneous solid, *J. Appl. Phys.* **1949**, *20*, 518-525.
32. Brumberger H.; Debye, P.; Anderson, H. R. Scattering by an inhomogeneous solid 2: the correlation function and its application, *J. Appl. Phys.* **1957**, *28*, 679-683.

33. Teubner, M.; Strey, R. Origin of the scattering peak in microemulsions, *J. Chem. Phys.* **1987**, *87*, 3195-3200.

34. Jinnai, H.; Hashimoto, T.; Lee, D.; Chen, S. H. Morphological characterization of bicontinuous phase-separated polymer blends and one-phase microemulsions, *Macromolecules* **1997**, *30*, 130-136.

35. Jinnai, H.; Nishikawa, Y.; Chen, S. H.; Koizumi, S.; Hashimoto, T. Morphological characterization of bicontinuous structures in polymer blends and microemulsions by the inverse-clipping method in the context of the clipped-random-wave model, *Phys. Rev. E* **2000**, *61*, 6773-6780.

36. Narimani, R.; Yang, A. C. C.; Tsang, E. M. W.; Rubatat, L.; Holdcroft, S.; Frisken, B. J. Controlling water content and proton conductivity through copolymer morphology, *Macromolecules* **2013**, *46*, 9676-9687.

37. Pang, G.K.H; Baba-Kishi, K.Z; Patel, A. Topographic and phase-contrast imaging in atomic force microscopy, *Ultramicroscopy* **2000**, *81*, 35-40.